Journal of Materials Chemistry B

Accepted Manuscript

ROYAL SOCIETY OF CHEMISTRY

www.rsc.org/materialsB

Engineering highly stretchable lignin-based electrospun nanofibers for potential biomedical applications

Dan Kai[1*], Jiang Shan[1], Zhi Wei Low[2], Xian Jun Loh[1,2,3*]

* Corresponding Author

[1]Institute of Materials Research and Engineering (IMRE), A*STAR, 3 Research Link, Singapore 117602, Singapore

[2]Department of Materials Science and Engineering, National University of Singapore, 9 Engineering Drive 1, Singapore 117576, Singapore

[3]Singapore Eye Research Institute, 11 Third Hospital Avenue, Singapore 168751, Singapore

E-mail: kaid@imre.a-star.edu.sg, lohxj@imre.a-star.edu.sg

Abstract

Lignin, one of the most abundant biopolymers on Earth, has been recognized as a renewable alternative to traditional petroleum-based plastics. The integration of lignin with synthetic and engineering plastics is an important approach to develop sustainable polymers. However, it is challenging to blend lignin with other polymers due to its brittle nature and poor dispersion in many composites. In order to improve the miscibility and compatibility of lignin with other plastics, a series of poly(methyl methacrylate) (PMMA) grafted lignin copolymers were prepared from atom transfer radical polymerization. The chain length of PMMA oligomers and glass transition temperature of the lignin copolymers was controlled by varying of lignin : methyl methacrylate ratio. The lignin mass fractions in the copolymers varied from 5.6% to 46.1%. These lignin-PMMA copolymers were further blended with poly(ε-caprolactone) (PCL) and engineered into nanofibrous composites by electrospinning. Tensile test and dynamical mechanical analysis showed that the incorporation of lignin-PMMA copolymers significantly improved the tensile strength, Young's modulus, and storage modulus of the resulting nanofibrous composites. The length of PMMA chain played a crucial role for the miscibility of lignin in PCL, and therefore enhanced the stiffness and ultimate elongation of the resulting nanofibers. Cell culture studies suggested that these PCL/lignin-PMMA nanofibers were biocompatible and promoted the proliferation, attachment and interactions of human dermal fibroblasts. With reinforced mechanical properties and good biocompatibility, these green and stretchable electrospun nanofibers are potentially useful as biomaterial substrates for biomedical application.

Keywords: Biomass, Sustainability, Mechanical reinforcement, Atom transfer radical polymerization, Biocompatibility

1. Introduction

It has been widely recognized that the integration of biomass polymers with synthetic and engineering plastics is important in the reduction of the consumption of petroleum-based materials as well as to develop sustainable polymers [1-6]. Lignin is a naturally derived biomacromolecule that exists in the cell wall of vascular plants, making it one of the most abundant natural polymers on Earth just after cellulose. Every year, more than 50 million tons of lignins are produced as a by-product of the papermaking industry. Besides its low cost and high availability, other properties of lignin, such as high carbon content, high thermal stability, biodegradability, antioxidant activity and favorable stiffness, have led to increasing interest in developing lignin into value-added products for industry applications [1, 3, 7]. However, due to the brittle nature of lignin and its incompatibility with some nonpolar polymeric systems, it is challenging to process and fabricate homogeneous and elastic lignin-based composites.

A potential strategy to blend lignin within a polymeric matrix is by grafting lignin of polymer chains that chemically identical or similar to the host polymer. Efforts have been made to graft polymers onto lignin by using free radical polymerization, condensation polymerization and even chemo-enzymatic approach [2, 7-12]. Atom transfer radical polymerization (ATRP) is one of the most widely used 'living' radical polymerization method to prepare polymers with different compositions, topologies and functionalities [13-17]. ATRP has proved to be an effective method to synthesize lignin-based copolymers, and multiple polymers, including poly(N-isopropylacrylamide) and polystyrene have been successfully grafted to lignin [18-20]. This polymerization technique also offers various benefits, such as the control of the molecular weight of grafted polymer chains and the number of polymer chain graft per macroinitiator.

Electrospinning is a simple and cost-effective processing technique to produce ultrafine polymeric micro/nanofibers in the form of a nonwoven membrane [21-23]. Electrospun membranes, possessing porous and fibrous architecture, high surface area to volume ratios, and unique mechanical properties, are promising for designing novel materials in a variety of application [24-27]. Several studies in the electrospinning of lignin with synthetic polymers, such as poly(ethylene oxide) (PEO) and poly(vinyl alcohol) (PVA) have been reported, but due to containing high amounts of brittle lignin their application was limited as a precursor for carbon fibers [28-30]. In this study, we synthesized a series of poly(methyl methacrylate) (PMMA) grafted lignin copolymers with different molecular weights via ATRP. Furthermore, these lignin-PMMA copolymers were blended with poly(ε-caprolactone) (PCL) and electrospun into composite nanofibrous membranes. A Food and Drug Administration (FDA) approved biodegradable synthetic PCL was chosen in our system because it shows good biocompatibility, good ductile and elastic properties and therefore has been utilized as a scaffold material for tissue engineering applications [22, 25]. Here we investigated the influence of the lignin-PMMA copolymers (with different molecular weights) on the topographical, mechanical properties, and biocompatibility of resulting nanofibers, exploring the potential of the PCL/lignin-PMMA nanofibers in biomedical application.

2. Materials and methods

2.1. Materials

All chemicals were purchased from Sigma-Aldrich Chemicals and used as received except where noted. Kraft lignin (M_n = 5000 g/mol, M_w = 28,000 g/mol) was dried at 105 °C overnight before use. Methyl methacrylate (MMA) monomer was run through a basic

alumina column before use to remove inhibitor. Copper(I) bromide (CuBr) was washed with ethanol before use.

2.2. Synthesis of lignin ATRP macroinitiators (lignin-Br)

The dried lignin (Alkali, 3.0 g, 0.6 mmol, contains –OH 22.3 mmol) was weighed in a reaction flask and cooled down to room temperature under nitrogen atmosphere. Subsequently, anhydrous *N,N*-dimethylacetamide (DMA, 30 ml) was injected into the flask to dissolve the lignin under stirring. Triethylamine (TEA, 53.5 mmol, 7.46 ml) was then added into lignin solution. After that, 10 ml of anhydrous DMA containing 2-bromoisobutyryl bromide (BIBB, 44.6 mmol, 5.51 ml) was added dropwise into the lignin solution under stirring over 2 hours in an ice-water bath. The mixture was allowed to react for 24 hours at room temperature. Then the reaction mixture was centrifuged and the supernatant was precipitated with 1000 ml of diethyl ether. The tan gel-like precipitate was re-dissolved into THF (50 ml) and the solution was then precipitated with 1000 ml of diethyl ether. The brown powder of lignin macroinitiator was collected and dried under vacuum at 40 °C. The number of initiator sites on lignin was determined by ^{1}H NMR (Supporting Information Fig. S1) in DMSO: δ (ppm) 1.4-2.2 (-CH_3 of initiation group), 3.5-4.3 (-CH_3O-), 6.0-8.0 (aromatic protons of lignin).

2.3. Synthesis of lignin-PMMA graft copolymers

In a typical example, lignin-Br (130 mg, 0.3 mmol Br), PMMA (1.5 g, 50 mmol), 1,1,4,7,10,10-hexamethyltriethylenetetramine (HMTETA, 83 mg, 0.36 mmol) and 10 ml of degassed acetone were added into a dry flask. The mixture was stirred at room temperature

and purged with dry nitrogen for 20 min. Then CuBr (43 mg, 0.3 mmol) was added and the mixture was purged with dry nitrogen for another 10 min at room temperature. The mixture was continued to stir for overnight at room temperature. After that, the experiment was stopped by opening the flask and exposing the catalyst to air. The final tan mixture was diluted with THF and passed through a short neutral Al_2O_3 column with THF as eluent to remove copper catalyst. The resulting eluate solution was concentrated to 10 ml and percipitated with 1000 ml hexane. The gray product, LM50, was collected by centrifugation and dried under vacuum at 40 °C. A series of lignin-PMMA graft copolymers with different compositions of PMMA were prepared under similar condition, as shown in Table 1.

2.4. Characterization of lignin-PMMA graft copolymers

Lignin, lignin-Br, lignin-PMMA were characterized by ^{1}H NMR (NMR (Bruker 400 MHz). Deuterated acetone and deuterated dimethyl sulfoxide (DMSO-d_6) were used as a solvent to dissolve synthesized materials.

Molecular weight and polydispersity index (PDI) of polymer samples were analysed by gel permeation chromatography (GPC, a Shimadzu SCL-10A and LC-8A system equipped with two Phenogel 5 μm 50 and 1000Å columns in series and a Shimadzu RID-10A refractive index detector). THF was used as eluent at a flow rate of 0.30 ml/min at 40 °C. Monodispersed poly(ethylene glycol) standards were used to obtain a calibration curve.

Thermogravimetric analysis (TGA) was carried out on a thermogravimetric analyser (Q500, TA Instruments, USA). Samples were heated at 20 °C/min from room temperature to 700 °C in a dynamic nitrogen atmosphere (flow rate = 60 ml/min).

Differential Scanning Calorimeter (DSC) thermal analysis was performed on a DSC (Q100, TA Instruments, USA) equipped with an autocool accessory and calibrated using indium. The following protocol was used for each sample: heating from room temperature to +180 °C at 20 °C/min, holding at +180 °C from 5 min, cooling from +180 °C to -20 °C at 20 °C/min, and finally reheating from -20 to +180 °C at 20 °C/min. Data were collected during the second heating run.

2.5 Electrospinning of nanofibers

A mixture of PCL and lignin-PMMA copolymers was dissolved in chloroform/methanol (75/25 in volume ratio), making the total concentration of 14% (w/v), and further stirred for 2 days. The homogeneous solutions were loaded into 5 ml plastic syringes fitted with a blunt 22-gauge needle. The syringe was then fixed horizontally on a syringe pump (KDS 100, KD Scientific, Holliston, MA) and the needle were connected to the positive electrode of a high voltage power supply (Gamma High Voltage Research). The feed rate of polymer solution was set at 0.5 ml/h, the applied voltage was 12 kV and tip to collector distance was 15 cm. Nanofibers were electrospun onto an aluminium foil wrapped collector or 15 mm cover slips. After spinning, the resulting fibers were dried overnight under vacuum and used for characterization and cell culture experiments. The detail compositions and denomination of PCL/lignin-PMMA nanofibers are shown in Table 2.

2.6 Characterization of nanofibers

The morphology of the PCL/lignin-PMMA nanofibers was investigated by scanning electron microscopy (SEM) (6360LA, JEOL, Japan). The diameters of the electrospun nanofibers

were determined from the SEM images using image analysis software (Image J, National Institutes of Health, VA). The average and standard deviation of the fiber diameter were calculated from 50 random measurements per image.

The thermal behaviors (melt temperature, T_m and thermal decomposition temperature, T_d) of PCL/lignin-PMMA nanofibers were carried out by DSC and TGA, and the procedures were the same as Section 2.4.

The tensile properties of the electrospun nanofibers were studied using a table top tensile tester (Instron 5943, Canton, USA) at a load cell capacity of 10 N. A segment of the nanofibers (5 × 30 mm, n = 6) was clamped at its cut for the axial testing. The thickness of the samples was about 150 μm, the gauge length was 20 mm, and the cross-head speed was set at 5 mm/min. Tensile strength, elongation and Young's modulus were calculated based on the stress–strain curve of each sample.

The viscoelastic properties of the electrospun nanofibers were measured in a Dynamic mechanical analyzer with a film tension clamp (15 mm gauge length). The samples have the thickness of ~150 μm and the width of ~5 mm. The test was carried out by heating the samples from 30 to 60°C at a heating rate of 3°C/min, oscillating amplitude of 1% strain and 1 Hz frequency.

2.7 *In vitro* cell culture

Electrospun nanofibers (on 15 mm cover slips) and tissue culture plates (TCP) were placed in 24-well plate while being pressed with stainless steel rings. The specimens were sterilized under UV light for 2 h, washed three times with PBS for 30 min each, and incubated in DMEM for 24 h before cell seeding. Then the specimens were seeded with human dermal

fibroblasts (HDFs) at a cell density of 5,000 cells per well. These cells were allowed to adhere overnight before changing medium, which was thereafter changed every 3 days.

Cell proliferation was monitored after 3, 6 and 9 days using MTT (3-(4,5-dimethylthiazol-2-yl)-2,5-diphenyltetrazolium bromide) assay. At each time point, 50 μL of sterile-filtered MTT stock solution in PBS (5 mg/mL) was added to each well, reaching a final MTT concentration of 0.5 mg/mL. After 4 h, the unreacted dye was removed by aspiration. The produced formazan crystals were dissolved in DMSO (500 μL/well). The absorbance was measured using a microplate reader (Infinite M200, Tecan) at wavelength of 570 nm.

Morphological study of HDFs cultured on different nanofibers was carried out after 7 days of cell culture by SEM. The cell-fiber constructs were rinsed three times with PBS and fixed in 3% glutaraldehyde for 3 h. The nanofibers were further rinsed in deionized water and dehydrated with increasing concentrations of ethanol (50%, 70% 90%, and 100%) for 15 min each. Finally, the cell-fiber constructs were treated with hexamethyldisilazane and air dried in a fume hood overnight.

To check the cytoskeleton, the cells were fixed with 2.5% paraformaldehyde for 30 min and permeated using 0.1% Triton X-100. Cells were further incubated with phalloidin FITC labelled (Life Technologies, Singapore) at a dilution of 1:100 in PBS for 90 min and counterstained with 4',6'-diamidino-2-phenylindole hydrochloride (DAPI) at room temperature. Samples were then mounted on glass slides using mounting medium and imaged with confocal laser scanning microscopy (Olympus Fluoview FV1000, Olympus Optical. Co., Ltd., Tokyo, Japan) at excitation wavelengths of 405 and 488 nm.

2.8 Statistical analysis

All the data presented are expressed as mean ± standard deviation of the mean. Student's t-test and one-way ANOVA were used, and differences between the groups are considered statistically significant at $p < 0.05$.

3. Results

3.1 Synthesis and characterization of lignin-PMMA copolymers

Natural lignin contains a large number of hydroxyl groups which are readily modified by BIBB through esterification reaction, and the modified lignin with created macro-initiation sites served as an excellent initiator for ATRP. Compared to the ^{1}H NMR spectra of raw lignin (Supporting Information Fig. S1), the modified lignin (lignin-Br) showed characteristic chemical shifts at 1.4-2.2 ppm corresponding to the methyl protons of the initiating sites, indicating the formation of 2-bromoisobutyryl ester on lignin. After calculation, it was found that the lignin-macroinitiator had 2.3 mmol of initiator sites per gram of material.

The PMMA-graft lignin copolymers were synthesized through ATRP reaction as shown in Scheme 1, and different ratios of MMA monomer were grafted onto lignin macroinitiator to form a 3D architecture composed of a lignin core and multiple arms of PMMA chains. Fig. 1 shows the ^{1}H NMR spectra of lignin-PMMA copolymer (LM50). Characteristic peaks of PMMA were shown at 0.8, 1.0 and 3.6 ppm corresponding to methyl protons, while the signals associated with the lignin aromatic ring (~7.2 ppm) and methoxyl groups (3.8 ppm) were also found in the spectra. As shown in Table 1, the unmodified lignin had a molecular weight of 5,000 and a high PDI of 5.6., while the copolymers showed tunable molecular weights varied according to the feed ratio of lignin : MMA. The M_n of copolymers increased from 10.8 kDa for LM30 to 88.7 kDa for LM100, while the average PMMA chain length increased from 5 for LM30 to 73 for LM100. Based on the molecular weight of lignin, the

mass fractions of lignin in the copolymers were calculated and ranged from 5.6% for LM100 to 46.1% for LM30. Therefore, both the NMR and GPC results demonstrate PMMA was successfully grafted on lignin cores.

The thermal properties of lignin and lignin-PMMA copolymers were characterized by DSC and TGA (Table 1 and Fig. 2). Unmodified lignin exhibited a high glass transition temperature (T_g) at 164 °C. PMMA grafted lignin copolymers showed dependence of T_g on the length of PMMA chains, and with the increase of PMMA chain length, T_g of the copolymers increased from 101 °C for LM30 to 131 °C for LM50. In the study of acrylic rosin polymer-grafted lignin composites, Wang et al. similarly found that T_g of the lignin composites highly depended on the length of alkyl side group [19]. The thermal stability of lignin and lignin-PMMA copolymers was investigated by TGA under N_2 atmosphere. The unmodified lignin thermally decomposed slowly with a very high char yield and showed 50% of the weight loss (thermal decomposition temperature, T_{d50}) at 670 ºC. It is a typical degradation curve for lignin due to the formation of residual pyrolyzed carbon materials. T_{d50} of the lignin-PMMA copolymers decreased with the grafted chain length of PMMA from 430 ºC for LM30 to 403 ºC for LM100 (Table 1). A neat PMMA showed the T_{d50} of 377 ºC (Supporting Information Fig. S2) and the relatively low decomposition temperature of PMMA chains resulted in the decreasing T_{d50} of the lignin-PMMA copolymers. LM30 and LM50, containing high contents of lignin, showed similar thermal decomposition curves to unmodified lignin, while LM70 and LM100 with much lower weight % of lignin exhibited one-stage catastrophic degradations at a derivative peak temperature of 410 ºC. Our result indicated that the grafting of lignin with PMMA generated new biomass-based thermoplastics, and T_g and T_d of the lignin composites are important parameters for the processing of lignin composites. The relatively high T_g and T_d suggests that typical sterilization methods such as autoclaving is suitable for the treatment of these materials prior to biomedical use.

3.2 Electrospinning of PCL/lignin-PMMA nanofibers

The morphology of PCL/lignin-PMMA nanofibers is shown in Fig. 3, and all the samples showed uniform randomly oriented bead-free nanofibrous networks. PCL fiber as control exhibited the largest fiber diameter of 1058 ± 261 nm. The addition of lignin-PMMA into PCL significantly reduced the fiber diameters and a higher concentration of lignin-PMMA copolymers resulted in a smaller fiber diameter. As shown in Table 2, the fiber diameters of PCL/LM70 decreased from 623 ± 112 nm for 25% of LM70 down to 370 ± 100 nm for 75% of LM70. On the other hand, there is no significant difference among the fiber diameters of PCL/LM30-50% (362 ± 62 nm), PCL/LM50-50% (551 ± 150 nm), PCL/LM70-50% (487 ± 107 nm) and PCL/LM100-50% (464 ± 75 nm), indicating that the length of PMMA chains did not significantly influence the fiber diameters of the electrospun membranes.

The thermal properties of PCL and PCL/lignin-PMMA nanofibers were characterized by DSC and TGA (Table 2). DSC results (Supporting Information Fig. S3) showed that the melt temperature (T_m) of PCL was 51 °C and all the PCL/lignin-PMMA nanofibers showed the similar T_m of ~51 °C, indicating that the addition of lignin-PMMA copolymers did not significantly affected T_m of the resulting nanofibers. On the other hand, TGA profiles (Supporting Information Fig. S4) revealed that blending lignin composites into PCL remarkably reduced thermal stability of the resulting nanofibers because of the lower T_d of lignin-PMMA copolymers, and T_d of PCL/lignin-PMMA nanofibers highly depended on the PMMA chain length and the concentration of lignin-PMMA copolymers. A high concentration of lignin-PMMA copolymers with a short PMMA chain length lead to a lower T_d due to the high content of lignin in the system.

3.3 Mechanical properties of PCL/lignin-PMMA nanofibers

The tensile test results of PCL/lignin-PMMA nanofibers are shown in Fig. 4 and Table 2. PCL fibers showed the tensile strength of 2.91 ± 0.29 MPa, Young's modulus of 7.6 ± 0.3 MPa and elongation at break of 278 ± 26 %. After blending of 50% lignin-PMMA copolymers, PCL/LM30-50 exhibited a significantly higher tensile strength of 3.84 ± 0.43 MPa (1.3 times) compared to neat PCL fibers, while other nanofibers showed comparable tensile strength values. Young's moduli of the electrospun nanofibers significantly increased with the addition of lignin-PMMA copolymers, and PCL/LM70-50 exhibited the highest Young's moduli of 44.4 ± 12.2 MPa (5.8 times compared to PCL).

Blending lignin into thermoplastics always leads to a dramatic drop of the ultimate elongation of the composites. In our study (Fig. 4A and Table 2), PCL/lignin-PMMA nanofibers (with 50% copolymers) showed significantly lower elongation at break compared to neat PCL fibers, but the ultimate elongation of every nanofibers was still more than 80%, which is desirable to be utilized as a biomaterial. It is also found that the elongation at break increased with the length of grafted PMMA chains from 84 ± 4 % for PCL/LM30-50 up to 118 ± 12 % for PCL/LM100-50, indicating that lignin copolymers with an appropriate grafted PMMA chain length could enhance the flexibility and elasticity of brittle polymer/lignin composites.

The influence of different amount of lignin-PMMA copolymers on the blend nanofibers was also investigated in this study. As shown in Fig. 4B, 25%, 50% and 75% LM70 was blended into PCL and electrospun into nanofibers. With the increasing concentration of LM70, the electrospun nanofibers exhibited an increasing Young's modulus but decreasing tensile strength and elongation at break. PCL/LM70-75 with 75% lignin copolymers showed the lowest tensile strength of 1.83 ± 0.19 MPa and elongation at break of 8 ± 3 %. In this system, 25% of PCL were not enough to form a matrix to support the 75% lignin-PMMA particles.

The extreme low elongation of PCL/LM70-75 presents the brittle nature of lignin copolymers, suggesting that electrospun nanofibers in this ratio are not suitable for biomedical application.

The viscoelastic properties of PCL/lignin-PMMA nanofibers were characterized by DMA under temperature sweep from 30 to 60°C at a heating rate of 3°C/min (1% strain and 1 Hz). Storage (G') and loss (G") moduli of each nanofibers are shown in Fig. 5. Neat PCL fibers exhibited the lowest G' (~8.7 MPa) and G" (~0.8 MPa) in the range of 30 to 60°C. In agreement with the results of Young's modulus, the addition of lignin-PMMA copolymers into PCL remarkably raised the G' of the blend nanofibers and a higher concentration of lignin copolymers resulted in higher G' and G" due to their ability to resist intermolecular slippage. (Fig. 5A). The addition of lignin-containing fillers resulting in increasing moduli of the resulting composites has been also observed by many other researchers. An increase in G' values with the increase of jute fibers content was reported in the study of high density PE/jute composites [31]. Alkylated lignin and wood flour were also found to improve the G' and stiffness of the PP composites [32, 33]. On the other hand, the effects of PMMA chain lengths on the viscoelastic properties of electrospun nanofibers were also investigated. As shown in Fig. 5B, the G' of PCL/lignin-PMMA nanofibers slightly decreased with the increasing length of PMMA chains, and PCL/LM100 showed the lowest G' among the three nanofibers. It is probably attributed to the lowest lignin content in PCL/LM100 as well as the enhanced mobility of longer PMMA chains in PCL matrix.

3.4 Biocompatibility of PCL/lignin-PMMA nanofibers

The proliferation capacity of HDFs on PCL and PCL/lignin-PMMA nanofibers over a period of 9 days were determined by an MTT assay. As shown in Fig. 6, the metabolic activities of HDFs on all the nanofibers were found to increase with culture time. At Day 3, cell

proliferation on each PCL/lignin-PMMA sample was significantly lower than that on PCL fibers (control). After 6 days of cell culture, the proliferation of HDFs on PCL/LM30-50 was found significantly higher than the cell proliferation on PCL and other PCL/lignin-PMMA nanofibers. Even after 9 days, cell proliferation on PCL/LM30-50 was still the highest among all the electrospun nanofibers. It might be attributed to the relative hydrophilicity of lignin (compared to PCL) and the advanced mechanical properties of PCL/LM30-50 nanofibers. As PCL/LM30-50 contained the highest amount of lignin, our results suggested the positive effects of the kraft lignin on the nanofibers for cell growth.

To understand the interaction of cell with lignin substrates, the morphology of HDFs grown on PCL and PCL/lignin-PMMA nanofibers after 7 days of culture was observed by SEM. As shown in Fig. 7 (and supporting information Fig. S5), cells grew and attached on the nanofibrous substrates upon proliferation. Higher numbers of cells were found attached on the PCL/LM30-50 fibers (Fig. 7B) compared to those on other nanofibers. Moreover, the cell phenotype was found more organized and stretched across on PCL/LM30-50 fibers than on pure PCL fibers (Fig. 7A). Unlike the cells on PCL with spindle or triangle shapes (a typical phenotype on a hydrophobic surface), the fibroblasts on PCL/LM30-50 fibers displayed a flat and thin shape, and were well spread to form an interconnected monolayer. HDFs grown on other PCL/lignin-PMMA nanofibers exhibited scattered and poorly spread, similar to those on PCL fibers. At a higher magnification, it is found that the pseudopods of HDFs on PCL/LM30-50 extended themselves with fiber orientation (Fig. 7E). In other words, the PCL/LM30-50 nanofibers promoted the extension of pseudopods, and therefore improved cell-material interactions as well as cellular interactions with each other. On the other hand, the pseudopod extension and cell-cell interactions were rarely observed on other nanofibers, which also explained the reason why PCL/LM30-50 nanofibers showed the highest cell proliferation.

The morphology and cytoskeletal architecture of the cells on different electrospun nanofibers were further evaluated after 7 days of culture by staining with phalloidin-FITC. As shown in Fig. 8 (and supporting information Fig. S6), HDFs, with prominent actin filaments, displayed different cytoskeletal architectures on different substrates. The cells on PCL exhibited a narrow spindle shaped morphology with a uniform distribution of F-actin. A high cell density and an organization of actin filaments were observed for PCL/LM30-50 nanofibers, and those cells showed a well-spread morphology with large numbers of stress fibers inside. As shown in Fig. 8E, actin filaments with the HDFs were organized into higher-order structures, forming bundles or three-dimensional networks along with the orientation of the nanofibers. Our results suggested that PCL/LM30-50 nanofibers promoted the crosslinking of actin filaments and stimulated filopodial protrusion, thereby enhancing the cell-cell communications on the nanofibrous substrates.

4. Discussion

Electrospinning is well suited for processing lignin-based materials into fibrous membranes, but the brittle nature of lignin greatly limited the application of the resulting products. PCL, a semicrystalline elastomer, was added into the systems to tailor the mechanical properties of the resulting nanofibers. Previous literature has shown that solvents play an important role in impacting the morphology of resulting electrospun fibers by affecting the viscosity, surface tension, conductivity and volatility of polymer solutions. Chloroform is the most commonly used solvent for electrospinning PCL due to its high solubility for the polymer. However, with this solvent PCL only produces microfibers (3-5 μm) instead of nanofibers [34]. To produce PCL-based nanofibers, some relatively highly toxic solvents such as dimethylformamide, dichloroethane, acetone and methylene chloride have been also reported [34-36]. In our system, polar solvent methanol was applied in order to stabilize the spray jet

during spinning to generate thinner and more homogeneous fibers. The addition of methanol in solution is also able to reduce the number of beads and prevent electrospraying [37]. In addition, varying the distance between needle tip and the collector also influences the fiber diameter and morphology [38, 39]. To obtain beadless fibers, a short distance can be applied only when a highly volatile solvent is used, while a longer distance would be a better choice for those solvents with low vapour pressure [40]. Moreover, a decrease in the tip-to-collector distance usually leads to the formation of wet fibers or the fibers with larger diameters [41]. Furthermore the shape of fibers changes from round to flat with the decreasing distance [41].

The matching of the mechanical properties of a biomaterial are important considerations for a biomedical application. For example, a tissue engineering scaffold with matching mechanical properties of the native tissue would promote cell attachment and differentiation, to provide mechanical integrity of the forming tissue and support an *in vivo* like mechanotransduction between the cells and their environment [42]. Fig. 4 shows the typical stress-strain curves of different PCL/lignin-PMMA electrospun nanofibers under tensile loading. Due to the random and interlacing arrangement of the fibrous network, every stress-strain curve of the nanofibers exhibits a linear region up to the proportionality limit followed by a non-linear segment, which was characterized by a considerable elongation without a corresponding increase in loading stress. As the applied tensile load needs to straighten the curved fibers and stretch the overlapping networks first before fibers break, electrospun nanofibrous membranes always show elasticity and flexibility compared to corresponding bulk materials. In our study lignin and its copolymers are brittle, so the ductile PCL was introduced into the system as matrix to enhance the elongation and flexibility of the resulting composites.

It is widely reported that lignin can be used as a filler for the reinforcement of plastic materials, such as polypropylene (PP) [43, 44], polyethylene (PE) [45, 46], polystyrene [47], poly(lactic acid) (PLA) [48, 49] and polyurethanes [7, 50] et al., but most materials, especially non-polar

polymers, showed weaker tensile strength or stiffness even with the addition of compatibilizers. Chen et al reported that both tensile properties and flexural properties of PP/lignin blends decrease with the increasing amount of lignin in PP, though the PP/lignin adhesion was improved by the alkylation of lignin. The tensile strength dropped from 33 MPa for neat PP down to 15 MPa for PP with 50% lignin, while Young's modulus reduced from 550 MPa for neat PP to 380 MPa for PP with 50% lignin [32]. Similar results were found in Alexy's study, and additionally they observed that the addition of lignin decreased the tensile strength of PE/lignin composites from 13.5 MPa for neat PE down to 5.8 MPa for PE with 30% lignin [51]. The study on blending cellulolytic enzyme lignin into PLA reported that the tensile strength of PLA blends fell from 63.8 MPa for neat PLA to 40.1 MPa for the blend with 40% lignin. However, here we firstly reported the reinforcement of electrospun PCL nanofibers by lignin copolymers (without any compatibilizer), and the PCL/LM30-50 nanofibers showed significantly higher tensile strength and Young's modulus even with 50% lignin copolymers (23% lignin content). The grafted PMMA chains on the lignin surface improved the interfacial binding between lignin particles and PCL matrix, and therefore favoring the miscibility and uniform dispersion of lignin. The enhanced interaction between star-shaped lignin-copolymers and PCL molecules resulted in a more efficient connectivity among PMMA-PCL binding points in each single nanofiber and hence raised the energy dissipation during fracture. Similarly, the graft polymerization of lactide onto lignin was reported to facilitate the dispersion of lignin-PLA copolymers in PLA matrix and hence resulted in an improved tensile properties of PLA/lignin composites [49].

Although many wood-based biopolymers, such as cellulose and its derivatives, have been developed into promising biomaterials for both tissue engineering and drug delivery, there are always doubts regarding the safety of lignin for potential applications in biomedical or healthcare fields. In our study, the biocompatibility of electrospun lignin nanofibers was

investigated using HDFs in order to predict their skin irritation potential. HDFs are skin cells within the dermis layer which are responsible for producing protein molecules, generating and maintaining the extracellular matrix as well as allowing the skin to recover from injury. Our results showed that PCL/LM30-50 nanofibers improved the proliferation and adhesion of HDFs. At present, few studies were conducted to evaluate the biocompatibility of lignins. The potential cytotoxic effects of lignins from different sources were evaluated by using the cell membrane integrity of human keratinocytes and murine fibroblast cells [52]. The IC_{50} (the dose inhibiting viability to 50%) results revealed that these lignins only showed cytotoxic at very high concentrations (more than 400 μg/ml). It was also reported that kraft lignin-based microcapsules were not cytotoxic and readily internalized into the cytoplasm of Chinese hamster ovary cells [53]. In a recent study, lignin/hydroxyapatite thin films were found to exhibit a good biocompatibility towards human mesenchymal stem cells [54]. Surprisingly, MTT results also showed that cell proliferation reduced with the increasing content of PMMA and PCL/LM100-50 exhibited the lowest proliferation values at all three time points. It indicated that a longer PMMA chain grafted on a lignin core might be slightly cytotoxic on human cells. These data are unexpected as PMMA is a Food and Drug Administration approved biomaterial for the application in biomedical field, such as contact lens and bone cements. Further study will be carried out to investigate this interesting result.

5. Conclusion

To overcome the brittle nature and poor dispersion of lignin in plastic composites, a series of lignin-based functional copolymers were synthesized with PMMA by ATRP. These green and sustainable copolymers exhibited tunable molecular weights and thermal properties easily controlled by varying of lignin : MMA ratio, holding a great potential as an alternative for petroleum-derived plastics. The lignin-PMMA copolymers displayed decreased T_g from

131 to 101 ºC with increasing lignin content from 5.6% to 46.1%. Furthermore, PCL/lignin-PMMA nanofibers were successfully prepared by electrospinning. The morphology and mechanical properties of the electrospun nanofibers were highly dependent on the contents of lignin copolymers and their PMMA chain lengths. PCL/LM30-50 containing 23% of lignin showed the reinforcement in tensile strength (+32%), Young's modulus (4 times) and storage modulus (4 times) compared to neat PCL. The PMMA grafted lignin copolymers with appropriate grafted chain lengths are potentially utilized as dispersion modifiers or fillers in biomass-based composite materials, enhancing their compatibility and mechanical properties. Moreover, the biocompatibility of the nanofibers was studied using HDFs, where the cells were found to attach, proliferate and interact well with the PCL/LM30-50 nanofibers. Our study shows that the potential applications of lignin-based nanofibers would be developed in biomedical and personal care fields.

Acknowledgements

This work was supported by the Institute of Materials Research and Engineering (IMRE), A*STAR (Agency for Science, Technology and Research), Singapore, and funded by the Science and Engineering Research Council (SERC) Personal Care Program.

References:

1. V. K. Thakur, M. K. Thakur, P. Raghavan and M. R. Kessler, *ACS Sustain. Chem. Eng.*, 2014, 2, 1072-1092.
2. J. H. Lora and W. G. Glasser, *J. Polym. Environ.*, 2002, 10, 39-48.
3. S. Laurichesse and L. Averous, *Prog. Polym. Sci.*, 2014, 39, 1266-1290.
4. H. Ye, C. Owh and X. J. Loh, *RSC Advances*, 2015, 5, 48720-48728.
5. X. J. Loh and Y.-L. Wu, *Chemical Communications*, 2015, DOI: 10.1039/C5CC03686K.
6. Z. Li and X. J. Loh, *Chemical Society Reviews*, 2015, 44, 2865-2879.
7. T. Saito, R. H. Brown, M. A. Hunt, D. L. Pickel, J. M. Pickel, J. M. Messman, F. S. Baker, M. Keller and A. K. Naskar, *Green Chem.*, 2012, 14, 3295-3303.
8. J. J. Meister and C. T. Li, *Macromolecules*, 1992, 25, 611-616.
9. Y. F. Huang, B. N. Zhao, G. Z. Zheng, S. J. He and J. Gao, *J. Appl. Polym. Sci.*, 1992, 45, 71-77.
10. C. Cui, H. Sadeghifar, S. Sen and D. S. Argyropoulos, *Bioresources*, 2013, 8, 864-886.
11. C. Mai, A. Majcherczyk and A. Huttermann, *Enzyme Microb. Technol.*, 2000, 27, 167-175.
12. C. Mai, O. Milstein and A. Huttermann, *Appl. Microbiol. Biotechnol.*, 1999, 51, 527-531.
13. X. J. Loh, *Journal of Applied Polymer Science*, 2013, 127, 992-1000.
14. X. J. Loh, S. J. Ong, Y. T. Tung and H. T. Choo, *Materials Science & Engineering C-Materials for Biological Applications*, 2013, 33, 4545-4550.
15. Z. F. Lin, S. Q. Cao, X. Y. Chen, W. Wu and J. S. Li, *Biomacromolecules*, 2013, 14, 2206-2214.
16. X. J. Loh, J. S. Gong, M. Sakuragi, T. Kitajima, M. Z. Liu, J. Li and Y. Ito, *Macromolecular Bioscience*, 2009, 9, 1069-1079.
17. X. J. Loh, W. C. D. Cheong, J. Li and Y. Ito, *Soft Matter*, 2009, 5, 2937-2946.
18. S. L. Hilburg, A. N. Elder, H. Chung, R. L. Ferebee, M. R. Bockstaller and N. R. Washburn, *Polymer*, 2014, 55, 995-1003.
19. J. F. Wang, K. J. Ya, A. L. Korich, S. G. Li, S. G. Ma, H. J. Ploehn, P. M. Iovine, C. P. Wang, F. X. Chu and C. B. Tang, *J. Polym. Sci. Pol. Chem.*, 2011, 49, 3728-3738.
20. Y. S. Kim and J. F. Kadla, *Biomacromolecules*, 2010, 11, 981-988.
21. D. Kai, G. Jin, M. P. Prabhakaran and S. Ramakrishna, *Biotechnol. J.*, 2013, 8, 59-72.
22. D. Kai, M. P. Prabhakaran, G. R. Jin and S. Ramakrishna, *Journal of Biomedical Materials Research, Part B-Applied Biomaterials*, 2011, 98B, 379-386.
23. N. Bhardwaj and S. C. Kundu, *Biotechnol Adv*, 2010, 28, 325-347.
24. D. Kai, M. P. Prabhakaran, B. Stahl, M. Eblenkamp, E. Wintermantel and S. Ramakrishna, *Nanotechnology*, 2012, 23, 10.
25. D. Kai, M. P. Prabhakaran, G. R. Jin and S. Ramakrishna, *Journal of Biomedical Materials Research, Part A*, 2011, 99A, 376-385.
26. D. Kai, Q. L. Wang, H. J. Wang, M. P. Prabhakaran, Y. Z. Zhang, Y. Z. Tan and S. Ramakrishna, *Acta Biomater.*, 2014, 10, 2727-2738.
27. D. Aussawasathien, J. H. Dong and L. Dai, *Synth. Met.*, 2005, 154, 37-40.
28. V. Poursorkhabi, A. K. Mohanty and M. Misra, *J. Appl. Polym. Sci.*, 2015, 132, 9.
29. S. X. Wang, L. P. Yang, L. P. Stubbs, X. Li and C. B. He, *ACS Appl. Mater. Interfaces*, 2013, 5, 12275-12282.
30. M. Ago, K. Okajima, J. E. Jakes, S. Park and O. J. Rojas, *Biomacromolecules*, 2012, 13, 918-926.
31. S. Mohanty, S. K. Verma and S. K. Nayak, *Compos. Sci. Technol.*, 2006, 66, 538-547.
32. F. Chen, H. H. Dai, X. L. Dong, J. T. Yang and M. Q. Zhong, *Polym. Compos.*, 2011, 32, 1019-1025.
33. M. Tajvidi, R. H. Falk and J. C. Hermanson, *J. Appl. Polym. Sci.*, 2006, 101, 4341-4349.
34. L. Van der Schueren, B. De Schoenmaker, O. I. Kalaoglu and K. De Clerck, *Eur. Polym. J.*, 2011, 47, 1256-1263.
35. X. H. Qin and D. Q. Wu, *J. Therm. Anal. Calorim.*, 2012, 107, 1007-1013.
36. A. G. Kanani and S. H. Bahrami, *J. Nanomater.*, 2011, DOI: 10.1155/2011/724153, 10.

37. P. Viswanathan, E. Themistou, K. Ngamkham, G. C. Reilly, S. P. Armes and G. Battaglia, *Biomacromolecules*, 2015, 16, 66-75.
38. Q. P. Pham, U. Sharma and A. G. Mikos, *Tissue Eng*, 2006, 12, 1197-1211.
39. C. Kriegel, A. Arrechi, K. Kit, D. J. McClements and J. Weiss, *Crit Rev Food Sci Nutr*, 2008, 48, 775-797.
40. N. Ashammakhi, A. Ndreu, A. M. Piras, L. Nikkola, T. Sindelar, H. Ylikauppila, A. Harlin, M. E. Gomes, N. M. Neves, E. Chiellini, F. Chiellini, V. Hasirci, H. Redl and R. L. Reis, *J. Nanosci. Nanotechnol.*, 2007, 7, 862-882.
41. T. Subbiah, G. S. Bhat, R. W. Tock, S. Pararneswaran and S. S. Ramkumar, *J. Appl. Polym. Sci.*, 2005, 96, 557-569.
42. X. Y. Chen, T. C. Chen, Z. F. Lin, X. E. Li, W. Wu and J. S. Li, *Chem. Commun.*, 2015, 51, 487-490.
43. X. Xu, Z. H. He, S. R. Lu, D. Guo and J. H. Yu, *Macromol. Res.*, 2014, 22, 1084-1089.
44. A. Gregorova, B. Kosikovka and A. Osvald, *Wood Res*, 2005, 50, 41-48.
45. R. R. N. Sailaja and M. V. Deepthi, *Mater. Des.*, 2010, 31, 4369-4379.
46. R. R. N. Sailaja, *Polym. Int.*, 2005, 54, 1589-1598.
47. R. Pucciariello, V. Villani, C. Bonini, M. D'Auria and T. Vetere, *Polymer*, 2004, 45, 4159-4169.
48. W. Z. Ouyang, Y. Huang, H. J. Luo and D. S. Wang, *J. Polym. Environ.*, 2012, 20, 1-9.
49. Y. L. Chung, J. V. Olsson, R. J. Li, C. W. Frank, R. M. Waymouth, S. L. Billington and E. S. Sattely, *ACS Sustain. Chem. Eng.*, 2013, 1, 1231-1238.
50. T. Saito, J. H. Perkins, D. C. Jackson, N. E. Trammel, M. A. Hunt and A. K. Naskar, *RSC Adv.*, 2013, 3, 21832-21840.
51. P. Alexy, B. Kosikova and G. Podstranska, *Polymer*, 2000, 41, 4901-4908.
52. V. Ugartondo, M. Mitjans and M. P. Vinardell, *Bioresour. Technol.*, 2008, 99, 6683-6687.
53. M. Tortora, F. Cavalieri, P. Mosesso, F. Ciaffardini, F. Melone and C. Crestini, *Biomacromolecules*, 2014, 15, 1634-1643.
54. A. Jankovic, S. Erakovic, C. Ristoscu, N. Mihailescu, L. Duta, A. Visan, G. E. Stan, A. C. Popa, M. A. Husanu, C. R. Luculescu, V. V. Srdic, D. Janackovic, V. Miskovic-Stankovic, C. Bleotu, M. C. Chifiriuc and I. N. Mihailescu, *J. Mater. Sci.-Mater. Med.*, 2015, 26, 14.

Scheme 1 Synthetic route for lignin-PEGMA copolymers

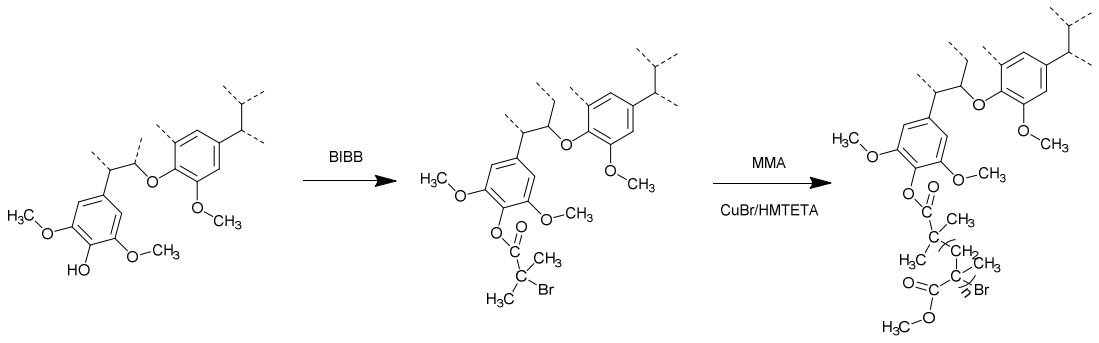

Fig. 1 ^{1}H of NMR spectra of the lignin-PMMA copolymer (LM 50 containing 31.4% of lignin) in acetone-d_6.

Fig. 2 (A) DSC and (B) TGA curves of lignin and lignin-PMMA copolymers.

Fig. 3 SEM images of electrospun (A) PCL, (B) PCL/LM30-50, (C) PCL/LM50-50, (D) PCL/LM70-50, (E) PCL/LM100-50, (F) PCL/LM70-25, (G) PCL/LM70-75 nanofibers. The scale bar = 10 μm.

Fig. 4 Typical stress-strain curves of PCL and PCL/lignin-PMMA nanofibers by tensile test (5 mm/min). (A) The comparison of nanofibers containing 50% of different lignin-PMMA copolymers and (B) the comparison of nanofibers containing different amounts of LM70.

Fig. 5 Storage (G', solid symbols) and loss (G", open symbols) moduli vs temperature of PCL and PCL/lignin-PMMA nanofibers by dynamic mechanical analysis (DMA, 1% strain and 1 Hz). (A) The comparison of nanofibers containing different amounts of LM70 and (B) the comparison of nanofibers containing 50% of different lignin-PMMA copolymers.

Fig. 6 Proliferation of human dermal fibroblasts on PCL and PCL/lignin-PMMA nanofibers, as determined by MTT assay. * $p < 0.05$ compared to PCL fibers at each time point; # $p < 0.05$ compared to PCL/LM30-50 fibers at each time point.

Fig. 7 Morphology of human dermal fibroblasts on electrospun nanofibers (A, D) PCL, (B, E) PCL/LM30-50, (C, F) PCL/LM100-50 after 7 days of culture. D to F are the corresponding images of A to C at a higher magnification, showing the interactions between cells.

Fig. 8 Laser scanning confocal microscopic images of human dermal fibroblasts on electrospun nanofibers (A, D) PCL, (B, E) PCL/LM30-50, (C, F) PCL/LM100-50 immunostained for F-actin (Green) and nuclei (Blue). D to F are the images merged with differential interference contrast images, showing the orientations of nanofibers. Scale bar = 30 μm.

Table 1 Molecular characteristics and thermal properties of lignin-PMMA copolymers

Polymers	Feed ratio [Br]:[MMA]	Theoretical M_n (g/mol)	M_n [a] (g/mol)	M_w [a] (g/mol)	PDI [a]	Average PMMA chain length [b]	Yield (%)	Mass% of lignin [c]	T_g [d] (ºC)	T_{d50} [e] (ºC)
Lignin			5,000	28,000	5.60				164	670
LM30	1:30	39,500	10,800	16,100	1.36	5	22.3	46.1%	101	430
LM50	1:50	62,500	15,900	25,300	1.59	9	23.8	31.4%	102	416
LM70	1:70	85,500	78,400	100,700	1.28	64	70.7	6.4%	129	407
LM100	1:100	120,000	88,700	106,800	1.20	73	66.9	5.6%	131	403

[a)]Determined by GPC. [b)]Determined by GPC based on the molecule weight of lignin (5,000 g/mol) and MMA (100 g/mol) as well as the content of Br in lignin macroinitiator (2.3 mmol/g) [c)]Determined by GPC based on the molecule weight of lignin (5,000 g/mol). [d)]T_g is glass transition temperature determinated by DSC. [e)]T_{d50}, thermal decomposition temperature, is defined as the temperature at which the mass of the sample is 50% less than its mass measured at 50°C (determinated by TGA). T_{d50} of neat PMMA is 377°C as control.

Table 2 Composition, fiber diameter, thermal and mechanical properties of electrospun nanofibers

Fibers	Copolymer type, %[a] (w/w)	Fiber diameter (nm)	T_m [b] (ºC)	T_d [c] (ºC)	Tensile strength (MPa)	Young's Modulus (MPa)	Elongation at Break (%)
PCL	N.A.	1058 ± 261	51	360	2.91 ± 0.29	7.6 ± 0.3	278 ± 26
PCL/LM30-50	LM30, 50%	362 ± 62*	49	240	3.84 ± 0.43*	30.5 ± 3.2*	84 ± 4*
PCL/LM50-50	LM50, 50%	551 ± 150*	51	252	2.68 ± 0.11	30.5 ± 0.4*	92 ± 3*
PCL/LM70-50	LM70, 50%	487 ± 107*	51	318	2.60 ± 0.27	44.4 ± 12.2*	104 ± 10*
PCL/LM100-50	LM100, 50%	464 ± 75*	51	314	2.61 ± 0.24	38.3 ± 1.7*	118 ± 12*
PCL/LM70-25	LM70, 25%	623 ± 112*	52	342	2.25 ± 0.22*	20.6 ± 1.1*	123 ± 16*
PCL/LM70-75	LM70, 75%	370 ± 100*	48	306	1.83 ± 0.19*	67.4 ± 4.5*	8 ± 3*

[a)]With respect to PCL. [b)]T_m is melt temperature determinated by DSC. [c)]T_d, thermal decomposition temperature, is defined as the temperature at which the mass of the sample is 5% less than its mass measured at 50°C (determinated by TGA). *Significantly different from corresponding parameters of PCL fibers ($p < 0.05$).

Fig. 1 ^{1}H of NMR spectra of the lignin-PMMA copolymer (LM 50 containing 31.4% of lignin) in acetone-d_6.

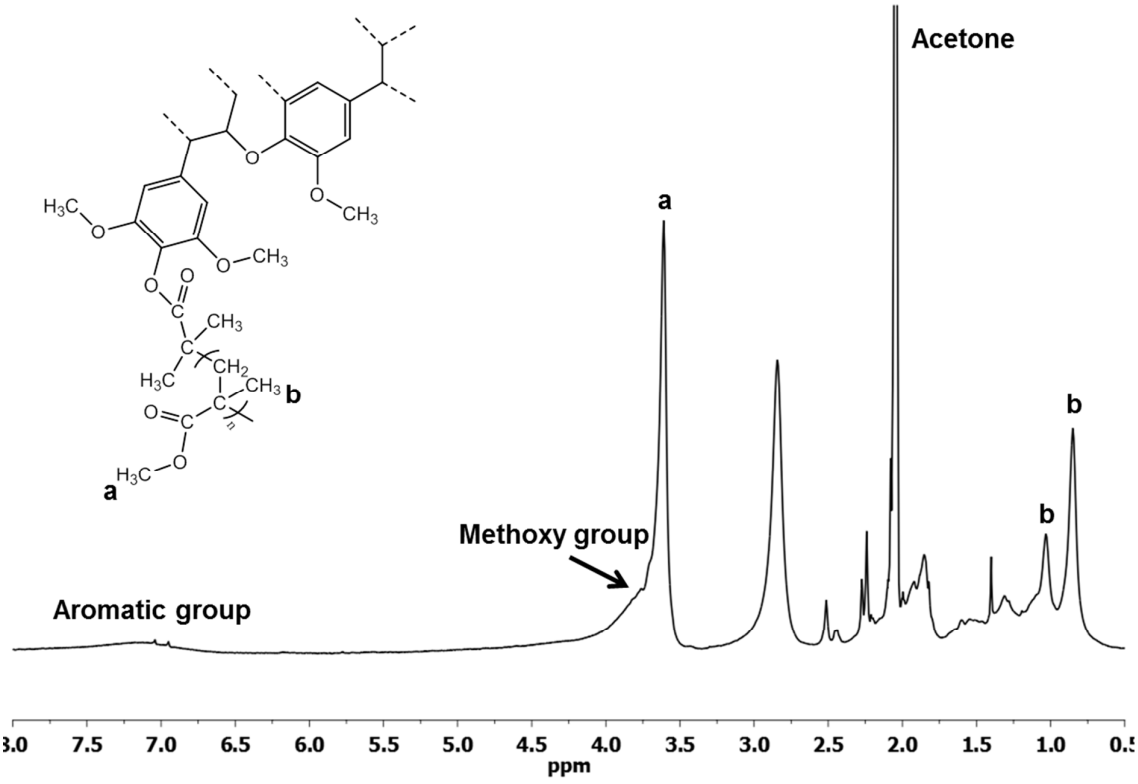

Fig. 2 (A) DSC and (B) TGA curves of lignin and lignin-PMMA copolymers.

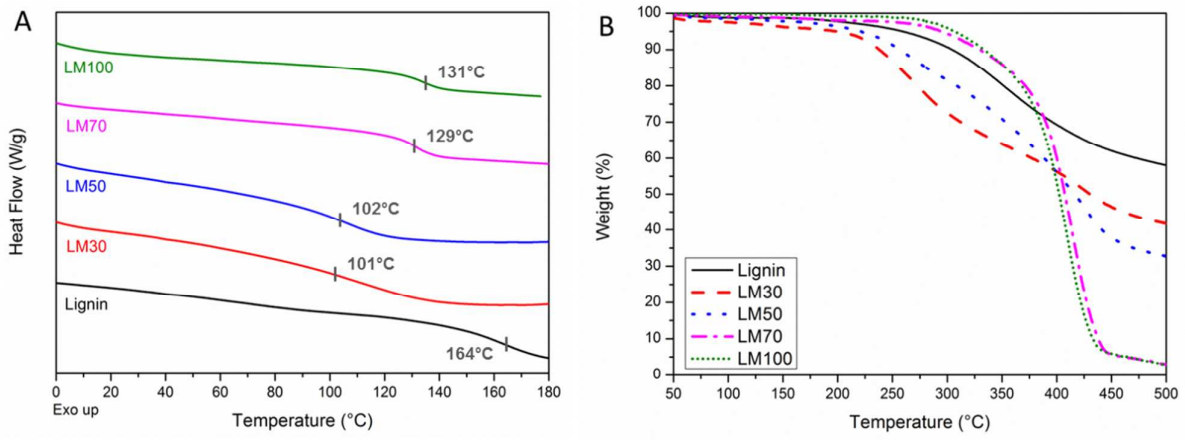

Fig. 3 SEM images of electrospun (A) PCL, (B) PCL/LM30-50, (C) PCL/LM50-50, (D) PCL/LM70-50, (E) PCL/LM100-50, (F) PCL/LM70-25, (G) PCL/LM70-75 nanofibers. The scale bar = 10 μm.

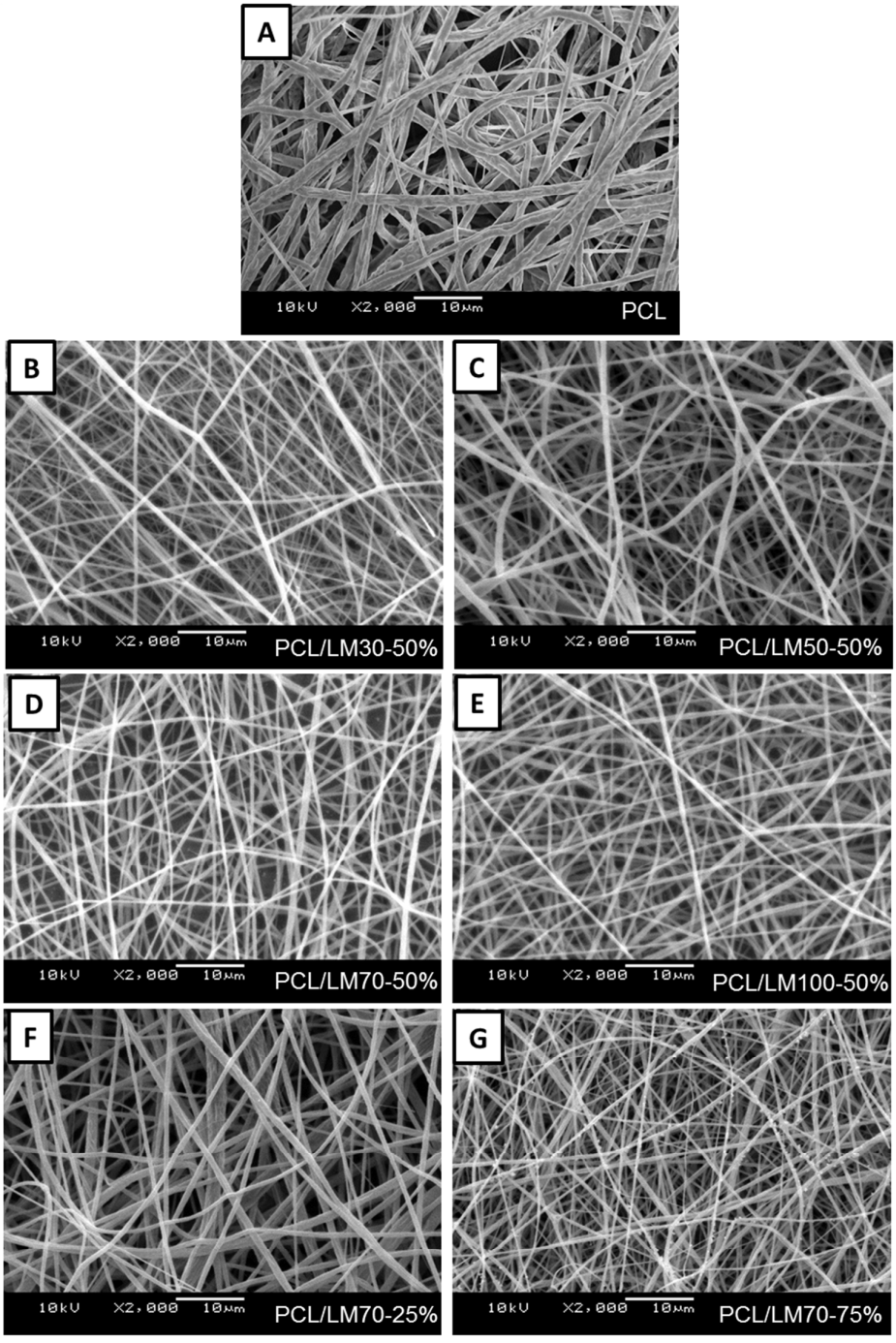

Fig. 4 Typical stress-strain curves of PCL and PCL/lignin-PMMA nanofibers by tensile test (5 mm/min). (A) The comparison of nanofibers containing 50% of different lignin-PMMA copolymers and (B) the comparison of nanofibers containing different amounts of LM70.

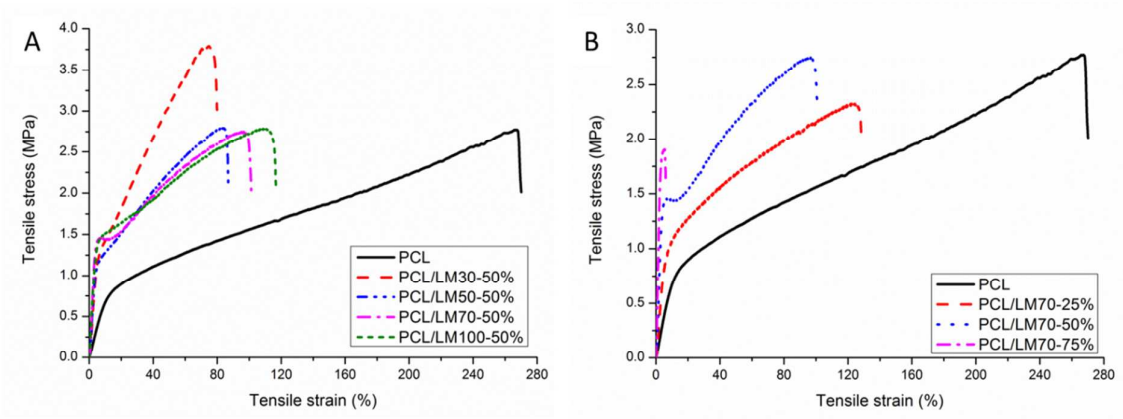

Fig. 5 Storage (G', solid symbols) and loss (G", open symbols) moduli vs temperature of PCL and PCL/lignin-PMMA nanofibers by dynamic mechanical analysis (DMA, 1% strain and 1 Hz). (A) The comparison of nanofibers containing different amounts of LM70 and (B) the comparison of nanofibers containing 50% of different lignin-PMMA copolymers.

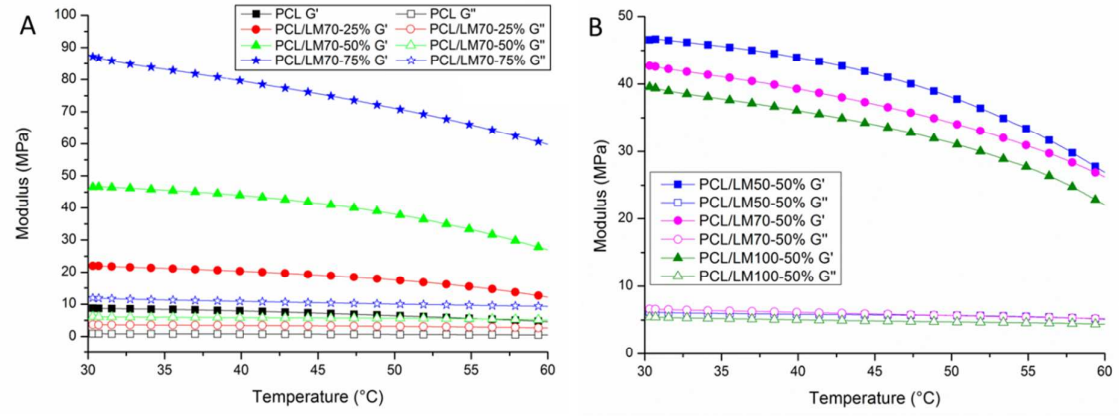

Fig. 6 Proliferation of human dermal fibroblasts on PCL and PCL/lignin-PMMA nanofibers, as determined by MTT assay. * $p < 0.05$ compared to PCL fibers at each time point; # $p < 0.05$ compared to PCL/LM30-50 fibers at each time point.

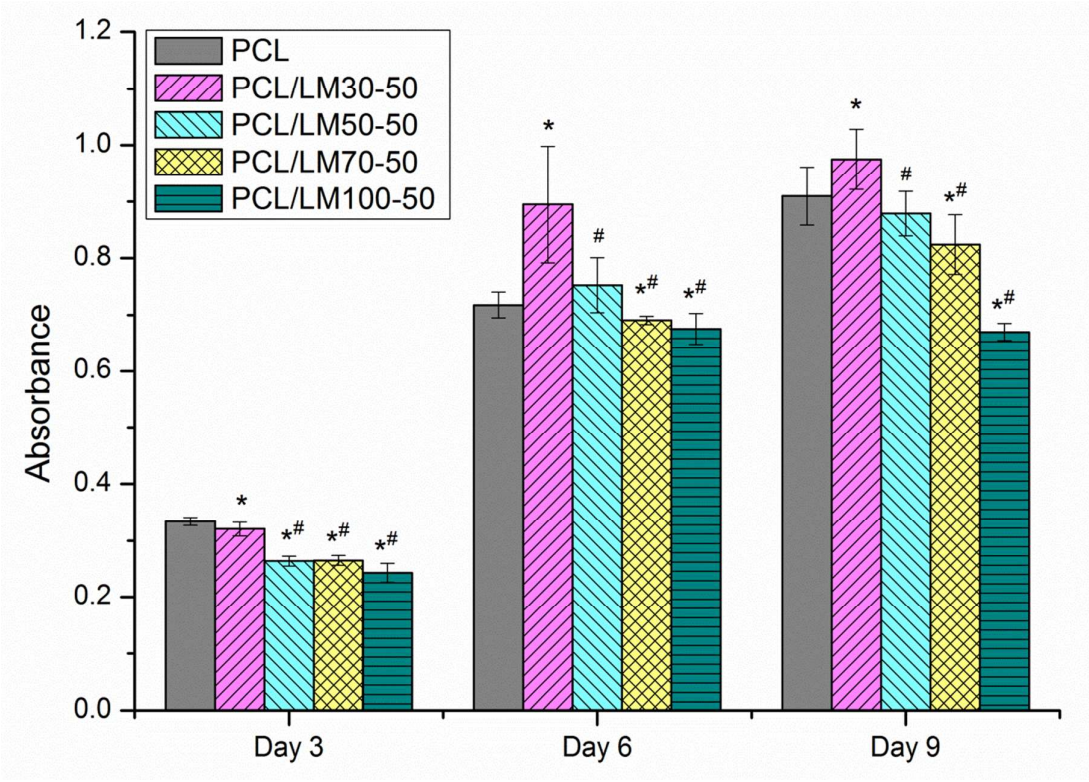

Fig. 7 Morphology of human dermal fibroblasts on electrospun nanofibers (A, D) PCL, (B, E) PCL/LM30-50, (C, F) PCL/LM100-50 after 7 days of culture. D to F are the corresponding images of A to C at a higher magnification, showing the interactions between cells.

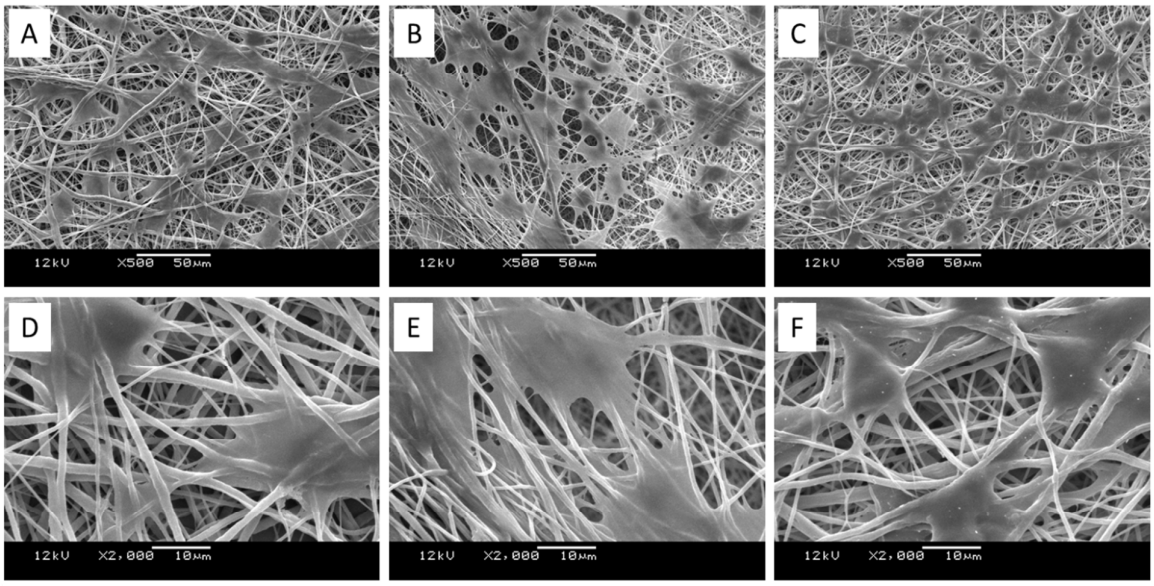

Fig. 8 Laser scanning confocal microscopic images of human dermal fibroblasts on electrospun nanofibers (A, D) PCL, (B, E) PCL/LM30-50, (C, F) PCL/LM100-50 immunostained for F-actin (Green) and nuclei (Blue). D to F are the images merged with differential interference contrast images, showing the orientations of nanofibers. Scale bar = 30 μm.

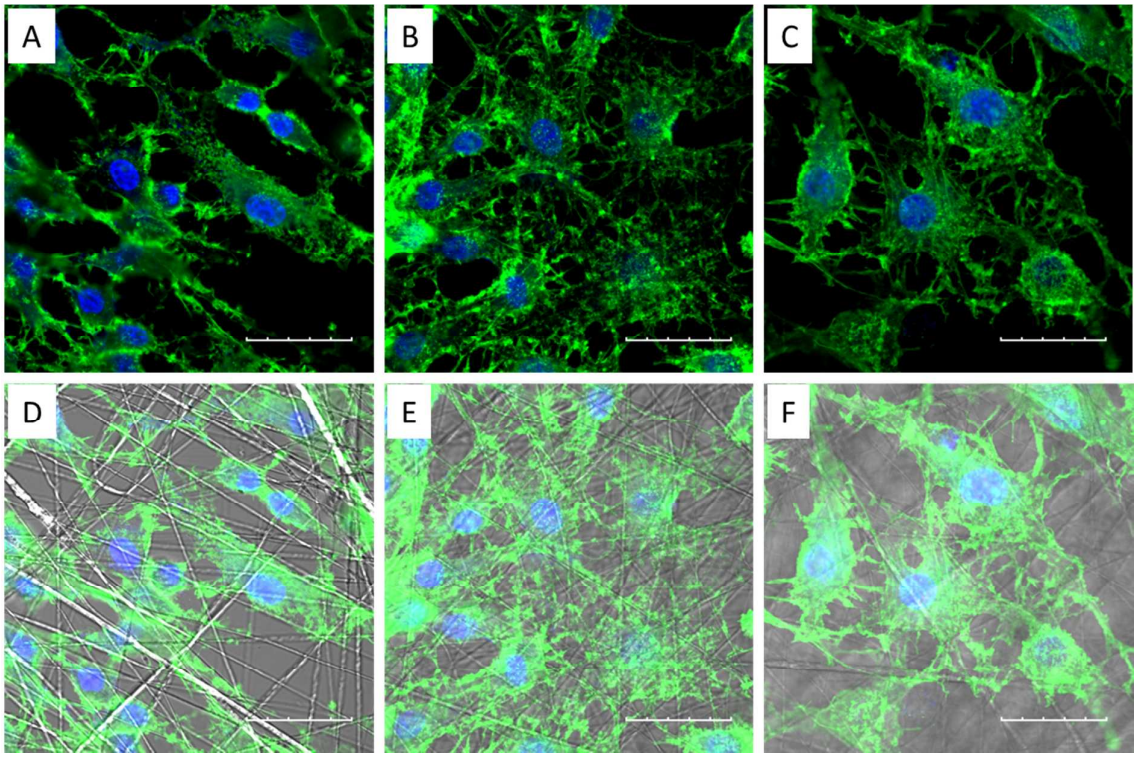

Contents entry

The incorporation of lignin-PMMA copolymers into PCL nanofibers significantly improved the mechanical properties and biocompatibility of the nanofibrous composites.